Chemical Engineering Journal 500 (2024) 156736

Contents lists available at ScienceDirect

Chemical Engineering Journal

journal homepage: www.elsevier.com/locate/cej

Assessing an electrochemical process for the treatment of tar-containing wastewater with hydrogen recovery

Nicola Melis, Laura Mais, Michele Mascia, Annalisa Vacca *

Dipartimento di Ingegneria Meccanica, Chimica e dei Materiali, Università degli Studi di Cagliari, Via Marengo 2, 09123 Cagliari, Italy

ARTICLE INFO

Keywords:
EAOP
Alkaline electrolysis
Energy consumption
Biomass gasification

ABSTRACT

Biomass gasification generates syngas with low carbon emissions but produces tar-contaminated wastewater that challenges environmental sustainability. This study explored using an alkaline electrolysis process with a DSA anode to remove organic pollutants from the effluent of a wet scrubber in a biomass gasification plant's syngas clean-up system. The effect of current density (16, 80, 160 mA cm^{-2}), area-to-volume ratio (0.03 and 0.15 cm^{-1}), and organic load on the process performances was assessed by monitoring total organic carbon, chemical oxygen demand and UV–Vis analyses; the phenolic fraction was also analysed with 4-aminoantipyrine colorimetric method. A kinetic analysis with zero-order and *pseudo*-first-order kinetic models was done for the relevant parameters, and the kinetic constants (k_{app}) were evaluated under all the explored conditions.

Results showed lower organic loads (higher dilution), as well as increasing current densities, have a beneficial effect on the phenol removal and mineralisation, achieving up to 50 % mineralisation in 8 h with 1:100 wastewater at 160 mA cm^{-2} and 0.15 cm^{-1}. Also, reducing the area-to-volume ratio leads to slower mineralisation processes. On the other hand, adopting low current densities with high organic loads lead to 100 % instantaneous current efficiency, in which the oxygen evolution reaction is fully suppressed, and pure hydrogen is produced. Insights into the economic aspects of the process in terms of energy per order and energy per mass were given: the energy consumption for the most favourable condition is 15.95 kWh kg^{-1}, corresponding to 960 kWh m^{-3} and a total cost of 72 € m^{-3}.

1. Introduction

Replacing fossil with renewable sources is critical, as the 2030 climate target of the EU recommends a reduction of at least 55 % in gas emissions from energy, industry, and transport, and set the climate neutrality by 2050 [1]. Combustion of fossil fuels to obtain energy is the largest source of CO_2 emissions [2], but the full replacement of fossil-based with renewable energies requires suitable carriers at least in high temperature applications. Hydrogen [3] is an extremely appealing carbon-free energy carrier as its combustion produces only water. Nevertheless, hydrogen is overwhelmingly obtained from non-renewable sources, and 830 million tons of CO_2 were released in 2020 for hydrogen production [4]. Thus, developing hydrogen production from clean and sustainable sources is crucial to achieving the European Green Deal [5].

Biomass is defined as the biodegradable fraction of products, wastes and residues originated from agriculture, forestry, fisheries, and related industries, as well as from municipal wastes. These products can be converted into hydrogen and syngas by biological or thermochemical processes, such as gasification, which is one of the most effective processes in terms of conversion efficiency [6]. Gasification uses steam and oxygen to convert biomass to syngas without combustion. The syngas can be used for power generation due to its high heating power or it can be converted to chemicals and fuels. However, the syngas produced in the gasifier contains high amounts of impurities, including significant quantities of tar, soot, and ashes [7]. The purification of syngas is often accomplished with wet scrubbing, which generates large volumes of wastewaters containing mainly tar, posing significant challenges on the sustainable development of biomass gasification. Gasification also produces a solid phase, known as "char", that includes the unconverted organic fraction and the inert material present in the treated biomass [8].

Tar is a complex mixture of condensable hydrocarbons with molecular weight higher than benzene, and it usually contains phenols, other one-ring aromatic compounds, and polyaromatic compounds (PAHs) [9–11]. Attempts to classify the tar composition have been made by

* Corresponding author.
E-mail address: annalisa.vacca@unica.it (A. Vacca).

https://doi.org/10.1016/j.cej.2024.156736

Available online 15 October 2024

Evans and Milne in 1997 [12] and, more recently, by the Energy Research Centre of the Netherlands (ECN) [10]. Anyway, the actual composition of tar depends on several parameters including the nature of biomass feedstock and temperature. Temperatures below 500 °C mainly produce oxygenated organic compounds (vanillin, catechol, anisole, *etc.*), while higher temperatures promote dehydroxylation, demethoxylation and demethylation processes, resulting in the formation of more condensed, branched, and heteroatomic compounds. Thus, as the temperature increases, the formation of light and heavy PAHs can be observed [13]. These compounds have a significant impact on human health and environment due to their high toxicity and carcinogenicity [6,14,15].

New and green strategies are then necessary to treat tar-polluted wastewater and make the gasification of biomasses a more sustainable process. Electrochemical processes powered by renewable energy are among the greenest methods, as they are energy-driven and use electrons as green reactants [16–18]. Moreover, the anodic electrooxidation of organic pollutants can be strategically coupled with other reductive reactions, such as the formation of high-value chemicals at the cathode, so that the treatment can be seen as a valorisation process and wastewaters as raw materials [19,20].

Several case studies in the literature focus on the electrochemical removal of phenolic and aromatic compounds from wastewaters with high initial Chemical Oxygen Demand (COD) [21–23]. Rajkumar *et al.* reported electrolysis of phenol and cresol from industrial wastewaters under galvanostatic conditions (54 mA cm^{-2}) using a mixed metal oxides anode (TiO_2-RuO_2-IrO_2), where the electrochemical oxidation is mediated by the formation of chlorine-based oxidants, such as dissolved chlorine and hypochlorite ions [24]. The authors investigated effluents with COD ranging from 600 to 9000 mg dm^{-3}. Similar conditions were applied by Fajardo *et al.* with Ti/RuO_2 anodes and NaCl as electrolyte for the depuration of phenol-containing olive mill wastewater with a COD of 22650 mg dm^{-3}. With a current density of 119 mA cm^{-2}, the authors reported a complete removal of the total phenolic content and a 17.2 % of COD removal [25].

To the best of our knowledge, only few articles report on the electrochemical degradation processes of tar. Zhao *et al.* tested PbO_2 electrodes, highlighting the effect of the current densities, the pH, and the electrode gap on the degradation efficiency. Under the best tested conditions, with an initial COD of 5125 mg dm^{-3}, the authors achieved a 90.5 % COD removal ratio after 3.5 h of electrolysis at 3 A dm^{-2} (30 mA cm^{-2}) [26]. With the same purposes, Yu *et al.* developed a hydrophobic PbO_2 electrode modified with benzalacetone. This novel electrode was used as anode in a continuous cycle reactor at room temperature with a current density of 90 mA cm^{-2}, achieving a 92.39 % removal of the initial COD of 4987 mg dm^{-3} [27]. However, these studies mainly focus on the treatment of the wastewaters to reduce the COD load. Recently, the electrochemical oxidation of organics contained in polluted wastewaters has been proposed as alternative to OER with the aim to couple with the hydrogen evolution reaction (HER) for cost-effective H_2 production in alkaline electrolysers [28,29]. The main advantages of these coupling reactions have been reported by Chen *et al.* [28], and include three aspects as follows: i) some oxidation reactions can exhibit smaller anodic overpotentials than OER, reducing the overall energy cost for H_2 production; ii) oxygen evolution will be significantly inhibited, preventing the mixing of H_2 and O_2 in a membrane-less cell; iii) valuable chemicals may be produced at the anode.

In this work, an alkaline electrolysis process was applied to real tar-containing wastewater deriving from the wet scrubber of a biomass gasification plant, using a commercial Ti/RuO_2 (DSA, dimensionally stable anode) anode. DSA presents high stability and activity and can even operate for nearly 10 years at industrial current densities (0.15 – 0.70 A cm^{-2}) [30]. The kinetics for the removal of global parameters such as COD and Total Organic Carbon (TOC) were determined as a function of the operating conditions. Different values of the applied current density and the ratio between the anodic area and the volume of treated solution have been tested. From the removal rate of the COD the electrical energy consumption for the process have been evaluated. The aim of the work was to find the operating conditions to reach the 100 % of faradaic yield for the removal of the organics, where the OER is suppressed allowing to membrane-less electrolysis where pure hydrogen is the only gas generated.

2. Experimental

The wastewater used in the experiments originates from the scrubber of a syngas produced by gasification of mixed biomasses at a plant located in the south of Sardinia, Italy.

The gasifier operates in continuous mode, while the scrubbing system works in batch recirculating mode. The clean-up water is pumped from a reservoir tank to the scrubber and back in a closed loop with makeup. The pH of the recirculating water tends to acidify during the operation of the plant and is eventually alkalinised with concentrated KOH to enhance the solubility of the organic compounds and prevent the formation of precipitates inside pipes and pumps. The pH is not controlled, so it is allowed to vary from 5 to 10 [30]. The concentration of the pollutants in the clean-up water thus increases over time, and a solid phase build up on the bottom of the tank; when the concentration of pollutants reaches the maximum allowed for the operability of the process the tank is partially emptied and refilled with fresh water. Wastewater and solids are sent to the relevant treatment plants; samples of the wastewater have been alkalinised to pH = 13.5, filtered and used in this work.

Table 1 shows the main features of the wastewater used in the experiments, including pH and conductivity, TOC, COD, and phenolic content measured by 4-aminoantipyrine method (5530 APHA standard method).

The experiments were performed in an undivided three electrode cell under batch conditions. The cell consisted of a 0.25 dm^3 stirred glass tank immersed in a thermostatic bath at 25 ± 2 °C. The electrode materials were platinised titanium grids for the cathode and Ti/RuO_2 (DSA, provided by De Nora, Milan) for the anode. The grid of DSA (2.5x5 cm^2, void fraction 0.54) and the cathode were placed in the cell with an interelectrode gap of 1 cm. A saturated calomel electrode (SCE) was used as reference electrode. Two ratios of geometrical anodic area to volume of treated wastewater (a = A/V) were selected: 0.15 cm^{-1} and 0.03 cm^{-1}.

The experiments performed to measure the hydrogen produced during the electrolyses of tar wastewater, have been performed in a batch recirculated filter press cell. The scheme of the experimental system is reported in Fig. 1. The single compartment cell presented two parallel electrodes with an interelectrode gap of 0.4 cm, with an anodic area of 6.2 cm^2 and a ratio between the anodic area and the recirculating volume of wastewater of 0.03 cm^{-1}. Stainless steel (AISI 304) was used as cathode. The cell was inserted in a hydraulic circuit in which the electrolyte was pumped by a peristaltic pump from a reservoir to the cell and back in a closed loop. The system was sealed to avoid the leakage of produced gas, and the reservoir was connected with a volumeter to collect the gases produced at cathode and anode through water displacement method [31].

Galvanostatic electrolyses at current densities ranging from 16 to 160 mA cm^{-2} were carried out using an AUTOLAB PGSTAT302N (Metrohm, Switzerland) potentiostat/galvanostat controlled with the

Table 1
Main parameters of TAR-contaminated wastewater.

Parameter	Value
TOC *(mg dm^{-3})*	24,000
COD *(mg dm^{-3})*	60,000
Phenolic content *(mg dm^{-3})*	900–1000
pH	13.5
Conductivity *(mS cm^{-1})*	94.6

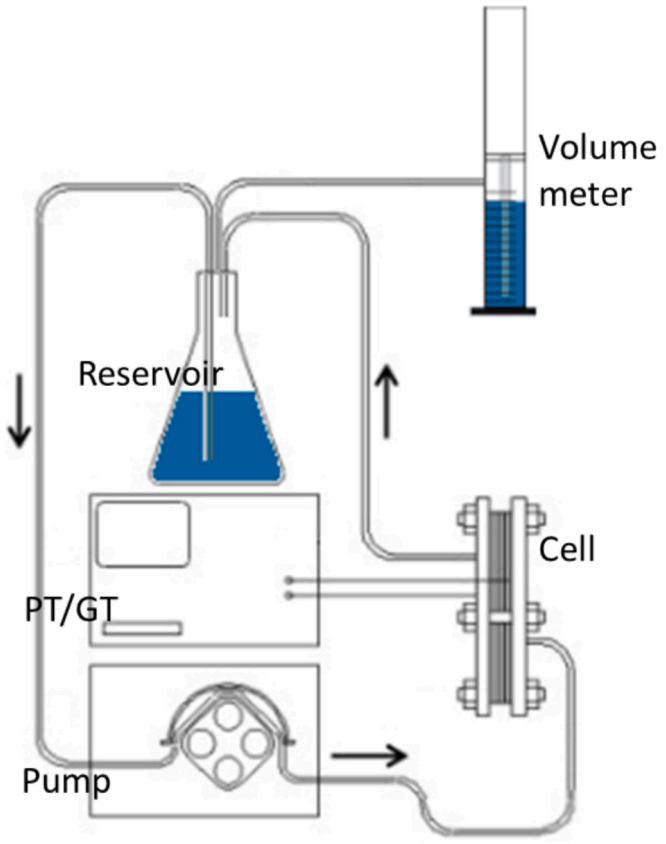

Fig. 1. Experimental system used for the electrolyses with hydrogen production measurements.

NOVA software.

The batch system used in these experiments was characterised in terms of anodic mass transfer coefficient k_m, which was estimated through the limiting-current technique using 0.1 M solution of potassium ferricyanide ($K_3Fe(CN)_6$, potassium hexacyanoferrate(III), 98 %, Alfa Aesar) and 1 mM solution of potassium ferrocyanide ($K_4Fe(CN)_6$, potassium hexacyanoferrate(II), 98.5 % Carlo Erba Reagents) in Na_2CO_3 0.5 M [32]. The k_m was calculated using the following equation (1):

$$k_m = \frac{I_{lim}}{C_0 nFA} \tag{1}$$

where C_0 is the concentration of ferrocyanide ions, I_{lim} is the limiting current value obtained from the polarization curves for the oxidation of ferrocyanide ions, n is the number of electrons, F is the Faraday constant and A is the geometrical area of the electrode.

During the runs, at regular intervals of time, samples of solution were withdrawn for the analyses.

The concentration of phenols in the samples was measured using the 4-aminoantipyrine (4-AAP) colorimetric method developed by Ettinger [33]. This method is based on the formation of a red-coloured complex between the 4-aminoantipyrine and the phenolic compound in the presence of an oxidant such as potassium hexacyanoferrate(III), $K_3Fe(CN)_6$, whose absorbance was measured at 510 nm using an Agilent spectrophotometer (Cary 60 UV–Vis). Since this method responds only to *orto*- and *meta*-substituted phenols, UV spectra of the samples were also monitored during the runs as a parameter representative of the organic content [34].

The trend of oxidation was monitored by measuring the COD of the samples using a pre-dosed test kit (GMSOLUTION SRL, COD 100–2000 mg dm^{-3}) analysed through a spectrophotometer Cary 60 UV–Vis. Total carbon (TC), inorganic carbon (IC) and TOC were measured using a Shimadzu TOC-L instrument.

The analytical determinations were used to calculate the instantaneous current efficiency (ICE) of the process. The ICE was calculated using the relation (2) [35]:

$$ICE = \frac{\Delta COD}{8I\Delta t}FV \tag{2}$$

where ΔCOD is the variation of the COD (mol O_2 dm^{-3}) related to the time interval Δt, I is the applied current intensity (A), F is the faradaic constant (C mol^{-1}), V is the volume of the electrolyte (dm^3) and 8 is the equivalent mass of oxygen.

Electrical energy per mass ($\mathbf{E_{EM}}$) and electrical energy per order ($\mathbf{E_{EO}}$) are selected as figures-of-merit to evaluate the electrical energy consumption for the process.[36] $\mathbf{E_{EM}}$ (kWh kg^{-1}), defined by equation (3), is reported to be most useful for high concentrations of pollutants, and it is typically applied for zero-order kinetics, as the removal rate of the contaminant is proportional to the current.

$$E_{EM} = \frac{Pt*10^6}{V\left(\gamma_i - \gamma_f\right)} \tag{3}$$

where P is the rated power (kW), V is the volume of treated wastewater (L), t is the treatment time (h) and γ is the mass concentration (mg L^{-1}).

On the other hand, $\mathbf{E_{EO}}$ (kWh m^{-3} $order^{-1}$) is best used when concentrations are low and for first-order kinetics, where the amount of energy required for the abatement of one order of magnitude of the contaminant is independent of its concentration. This figure of merit can be calculated using equation (4).

$$E_{EO} = \frac{38.4*P}{Vk'} \tag{4}$$

where P, and V have the same definitions as in $\mathbf{E_{EM}}$, and k' is the first-order rate constant (min^{-1}).

3. Results and discussion

Fig. 2 shows the polarisation curves obtained from linear sweep voltammetries (LSVs) at different scan rates with the wastewater. As a comparison, the figure also reports data obtained with two solutions: i) KOH at pH = 13.5 (the same pH value of the wastewater); ii) KOH at pH = 13.5 with 1000 mg dm^{-3} of phenol (the same concentration of the phenols in the wastewater).

The curves obtained with the wastewater show a current onset at less positive potential than that of the KOH solution, and an oxidation wave is well visible that can be related to a direct electron transfer between the pollutants and the electrode surface. At higher potentials the region of oxygen evolution reaction is well defined, and it overlaps with the curve related to KOH, indicating that the presence of organics did not hinder the OER.

As the scan rate increases, the shoulder at + 0.19 V slightly shift towards more positive potential.

Moreover, plotting the current density of the peak as a function of the scan rate (see inset of Fig. 2) a linear trend is observed that indicates a kinetic-controlled process with absorbed species onto the electrode surface [37]. The curve obtained with solutions containing phenol presents a similar trend, although the onset of current starts at more positive potential indicating the presence of components more oxidisable than phenol in the wastewater. Moreover, the oxidation peak for phenol is detected at higher potential than that of tar (around + 0.5 V): this can be attributed to the presence of substituted phenols and other derivatives, which are oxidised at less positive potential than phenol.

To better asses the kinetics of the different processes, galvanostatic electrolysis were performed with 1:10 or 1:100 diluted wastewater, and UV spectra were measured at different electrolysis times. Fig. 3 shows an example of UV spectra measured during the electrolysis at 160 mA cm^{-2}

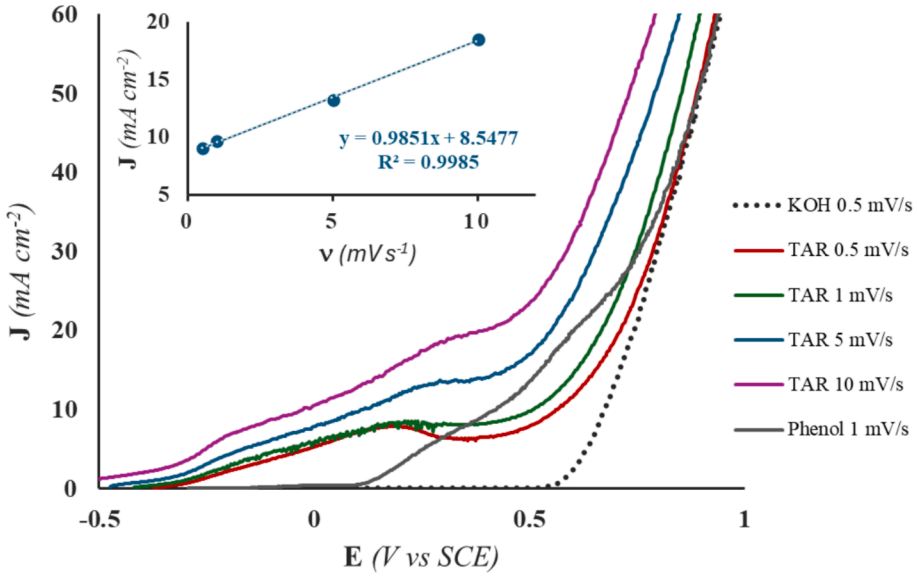

Fig. 2. LSV of KOH 0.2 M, 1000 ppm solution of phenol, and undiluted tar solution recorded at different scan rates. The inset shows the linear relation between the current density (J) and the scan rate (ν) of the oxidation peak at + 0.19 V in the undiluted tar solution.

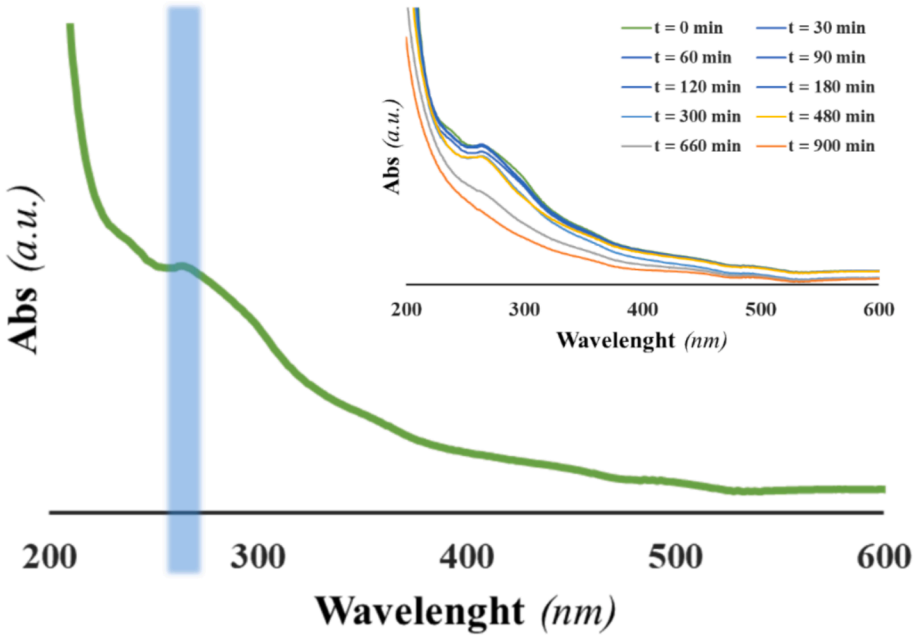

Fig. 3. Example of UV spectrum of tar wastewater (1:10 dilution). Inset shows the trend with time of UV spectra during the galvanostatic electrolysis at 16 mA cm^{-2}.

with 1:10 diluted wastewater (UV spectra of the other experiments are reported in **Fig. S1**). The initial spectrum is typical of a heterogeneous wastewater showing an increase of absorbance with decreasing wavelength and a lack of absorbance bands [34]. The shoulder in absorbance at 280 nm (UV_{280}) is related to organic matter containing π–π conjugated double bonds (*i.e.* C = C and C = O), and it has been chosen to represent the whole aromatic compounds content [38]. As shown in the inset of Fig. 3, UV_{280} decreased with time and finally disappeared, indicating the aromatic fraction was gradually removed. Of note, during the treatment, a discolouration of the wastewater from dark brown to pale yellow was also observed (see **Fig. S1e**).

Other than UV_{280}, phenol concentration was also analysed during the electrolyses, and decreasing trends of both parameters were observed, as shown in Fig. 4. As a comparison, the green dashed line shows the trend with time calculated for a mass transfer-controlled process with $a \bullet k_m = 9.1 \bullet 10^{-3}$ min^{-1}. The trend of UV_{280} overlaps that of phenol with 1:100 diluted wastewater, and both follow an exponential trend, with a specific reaction rate equal to the relevant mass transfer rate coefficient. With 1:10 dilution, the removal of phenol is mass transfer-controlled at high current density, while a linear trend of UV_{280} is observed in the initial region, followed by an exponential trend as the concentration decreases, confirming the controlling step depends on the organic load.

These considerations are further confirmed plotting the trend of the UV_{280} with the supplied charge (Fig. 4**c**). For 1:10 diluted wastewater the curves are overlapped at both levels of current densities in the initial region. At the highest applied current density, an exponential trend can be observed as the concentration decreases. The curves obtained with 1:100 diluted wastewater are not overlapped and follow an exponential decay, as it is expected for a mass transfer-controlled process.

These results indicate that under the conditions adopted in this set of

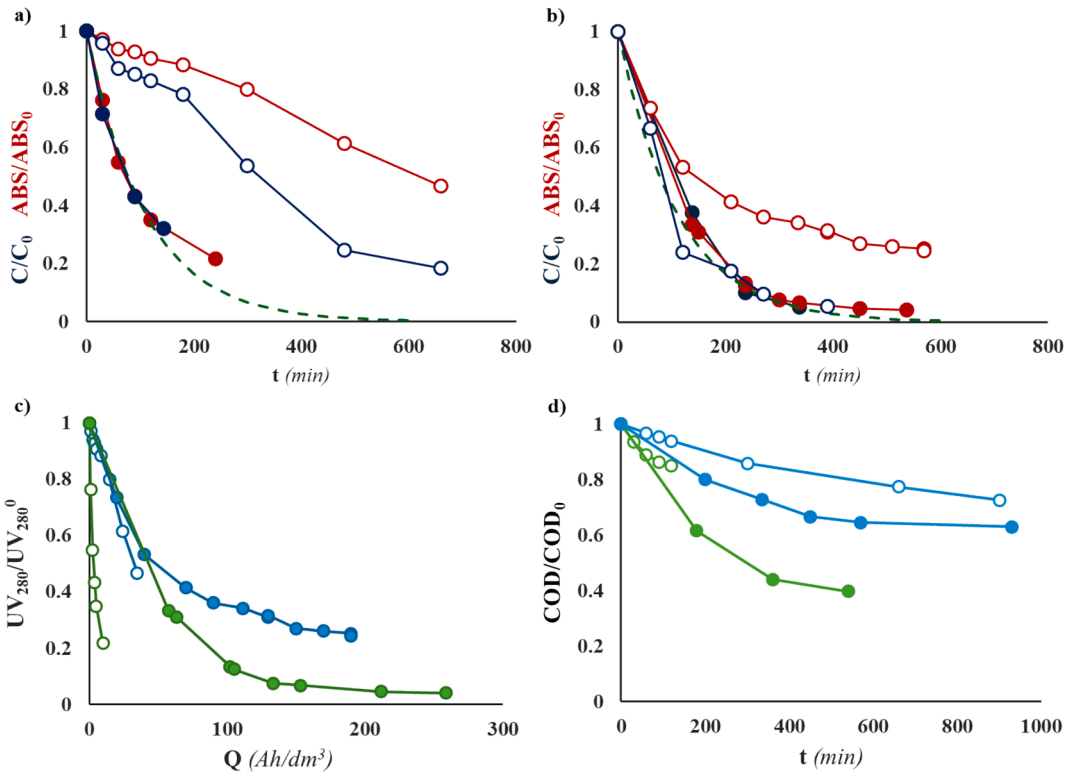

Fig. 4. a, b) Normalised trend of UV_{280} (red symbols) and phenol concentration (blue symbols) at two different electrolysis conditions (16 mA cm^{-2} in panel a, and 160 mA cm^{-2} in panel b) and two dilutions: 1:10 (empty symbols) and 1:100 (full symbols). The green dashed line shows the trend of a pure mass transfer-controlled process calculated with $a \bullet k_m = 9.1 \bullet 10^{-3}$ min^{-1}. **c)** Trend of UV_{280}/UV^0_{280} as a function of specific supplied charge for wastewater with dilution 1:10 (turquoise data) and dilution 1:100 (green data). J = 16 mA cm^{-2} (empty symbols) and J = 160 mA cm^{-2} (full symbols). **d)** Trend of normalised COD over time for the diluted solutions of tar (1:10 and 1:100) at two different current density (16 and 160 mA cm^{-2}).

experiments, the kinetics of phenols oxidation is mass transfer-controlled, while that of UV_{280} removal depends on the applied current density and the organic load. With 1:10 diluted wastewater the removal of UV_{280} is slower than that of phenol, while with 1:100-diluted wastewater at 160 mA cm^{-2}, also UV_{280} decreases without kinetic limitations. The COD removal rate (Fig. 4d) increased with the current density, but the relevant kinetic constants are slower than those calculated for UV_{280}, indicating the formation of non-aromatic byproducts that are resistant to the oxidation process. This behaviour was already observed in the literature, where sequential steps for the oxidation of aromatic compounds at DSA anodes have been observed with a first oxidative step that leads to the formation of cyclic intermediates, followed by a further oxidation of these byproducts to aliphatic acid and eventually CO_2 [39].

The degree of mineralisation has been assessed with TC, TOC, and IC measurements. As shown in Fig. 5, the TC is almost constant with time, while the TOC decreases indicating the conversion of the organic carbon into inorganic carbon-containing species. This can be ascribed to the alkaline pH of the wastewater that absorbs the carbon dioxide produced during the mineralization process, with a build-up of concentration of bicarbonates and carbonates. Moreover, with the 1:10 diluted wastewater at 16 mA cm^{-2}, it is observed a 30 % of TOC removal in 15 h. On the other hand, TOC starts at 218 mg dm^{-3} and decreases to 108 mg dm^{-3} after almost 500 min of electrolysis, thus achieving a 50 % of TOC mineralisation in roughly 8 h with the 1:100 diluted wastewater and 160 mA cm^{-2}.

Further experiments on the as received wastewater, were carried out at three current densities (16, 80, 160 mA cm^{-2}) and two different values of a (0.03 and 0.15 cm^{-1}). Fig. 6 shows the trend with time of UV_{280} and phenols normalised with their initial values. For both ***a***

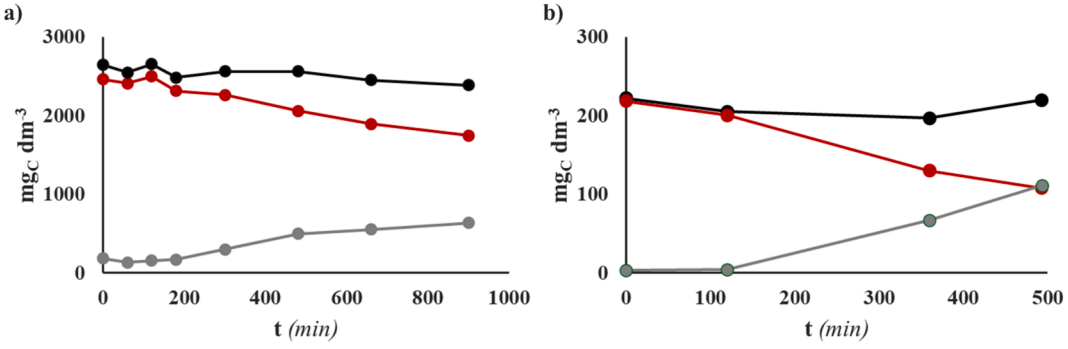

Fig. 5. TC (black dots), TOC (red dots) and IC (grey dots) reported against time of galvanostatic electrolysis for **a)** the 1:10 diluted solution at 16 mA cm^{-2}, and **b)** the 1:100 diluted solution at 160 mA cm^{-2}.

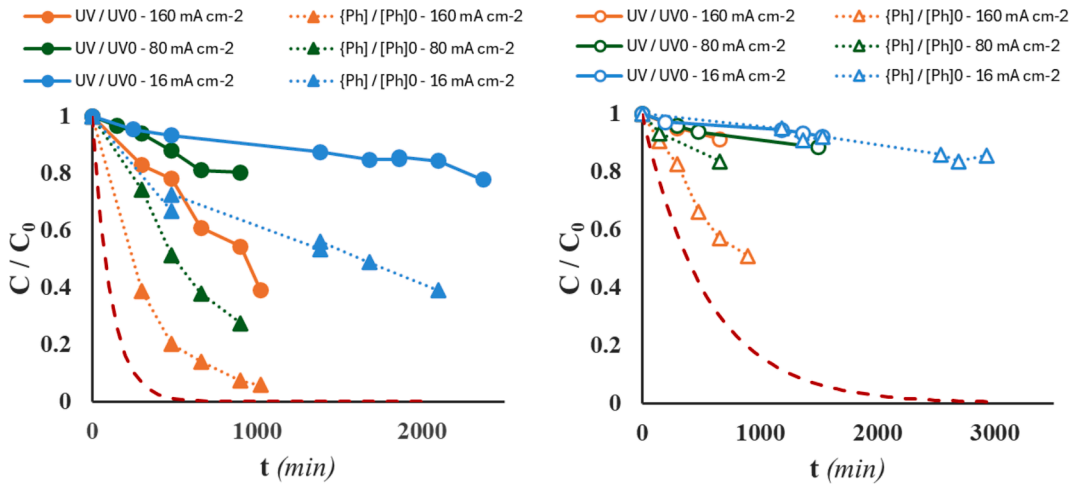

Fig. 6. Trends of normalised concentration (UV/UV^0_{280} and C_{Ph}/C^0_{Ph}) for the three current densities (16, 80, 160 mA cm^{-2}) at the two a ratio (0.15 cm-1 in panel a, and 0.03 cm-1 in panel b). The dashed red line in panels represents the curve for the corresponding $a \cdot k_m$: $9.1 \cdot 10^{-3}$ for a = 0.15 cm^{-1}, and $1.82 \cdot 10^{-3}$ for a = 0.03 cm^{-1}.

values, the calculated trend for a purely mass controlled process is reported as a dashed red curve ($a \bullet k_m = 9.1 \bullet 10^{-3}$ min^{-1} for $a = 0.15$, and $a \bullet k_m = 1.82 \bullet 10^{-3}$ min^{-1} for $a = 0.03$). As shown, also in this case the removal rates of phenols are faster than those of UV_{280} and follow an exponential decay, although the kinetics is not mass transfer-controlled. The trend of UV_{280} with time is linear, as it was observed in current-controlled processes; this is further confirmed by **Figure S2**, where the decrease of UV_{280} is reported as a function of the supplied charge.

The rate of UV_{280} decrease can be then described with a zero-order kinetics, while the removal of phenols follows a *pseudo*-first order kinetics. The two processes can be described with the equations **(5) and (6)** respectively:

$$\frac{C}{C_0} = 1 - k_{UV} t \quad (5)$$

$$ln\frac{C}{C_0} = -k_{Ph} t \quad (6)$$

The values of k_{UV} and k_{Ph} obtained by fitting the experimental data (see **Figure S3**) are reported in Table 2 with the relevant conditions. As shown, k_{UV} and k_{Ph} increase with the current density, moreover the value of k_{Ph} evaluated from the exponential decay of the concentration is lower than the mass transfer coefficients obtained under the same experimental conditions indicating a mixed controlled process.

The TOC removal obtained under these conditions are shown in Fig. 7, while Table 3 reports the relevant kinetic calculated with a *pseudo*-first-order kinetic model (equation **(6)**, as reported in **Figure S4a**. As it can be observed, the mineralisation increases with both current density and the *a*. Of note, all the kinetic constants related to the mineralisation are significantly lower than k_{UV}, indicating that the oxidation of the aromatic fraction leads to organic intermediates rather than CO_2.

The process was also monitored with COD analyses, whose

Table 2
Calculated kinetic constants for the decreasing of UV_{280}/UV^0_{280} and C_{Ph}/C^0_{Ph} of phenol in the explored conditions of Fig. 5.

Current Density (mA cm^{-2})	**a** (cm^{-1})	**k_{Ph}** (min^{-1})	**R^2**	**k_{UV}** (min^{-1})	**R^2**
16	0.03	$5.95 \bullet 10^{-5}$	0.987	$5.11 \bullet 10^{-5}$	0.937
80	0.03	$3.45 \bullet 10^{-4}$	0.990	$8.50 \bullet 10^{-5}$	0.929
160	0.03	$7.88 \bullet 10^{-4}$	0.993	$1.41 \bullet 10^{-4}$	0.980
16	0.15	$4.52 \bullet 10^{-4}$	0.979	$8.55 \bullet 10^{-5}$	0.947
80	0.15	$1.42 \bullet 10^{-3}$	0.995	$2.42 \bullet 10^{-4}$	0.960
160	0.15	$2.92 \bullet 10^{-3}$	0.993	$5.55 \bullet 10^{-4}$	0.974

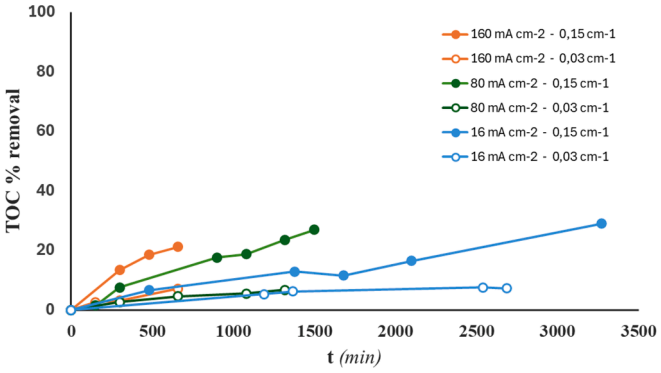

Fig. 7. Trend of TOC % removal over time for the three explored current densities at two a ratio.

Table 3
Calculated pseudo-first-order kinetic constants for the decreasing of TOC/TOC_0 (k_{TOC}) and COD/COD_0 (k_{COD}) in the explored conditions of Figs. 6 and 7, respectively.

Current Density (mA cm^{-2})	**a** (cm^{-1})	**k_{TOC}** (min^{-1})	**R^2**	**k_{COD}** (min^{-1})	**R^2**
16	0.03	$3.29 \bullet 10^{-5}$	0.956	$4.13 \bullet 10^{-5}$	0.999
80	0.03	$5.65 \bullet 10^{-5}$	0.979	$6.00 \bullet 10^{-5}$	0.983
160	0.03	$1.16 \bullet 10^{-4}$	0.985	$2.85 \bullet 10^{-4}$	0.986
16	0.15	$9.63 \bullet 10^{-5}$	0.983	$8.76 \bullet 10^{-5}$	0.942
80	0.15	$2.06 \bullet 10^{-4}$	0.997	$1.82 \bullet 10^{-4}$	0.983
160	0.15	$3.97 \bullet 10^{-4}$	0.988	$6.61 \bullet 10^{-4}$	0.989

normalised trend over time is reported in Fig. 8 for all the explored conditions. In this case as well the degradation has been quantified with a *pseudo*-first-order kinetic model (Table 3, **Figure S4b**). By comparing the two kinetic constants (k_{TOC} and the k_{COD}), it can be noted that the values are fairly similar at low current densities. However, at the highest current density, k_{COD} observed is roughly double that of k_{TOC}. Such result further confirms the formation of refractory intermediates that require higher current densities to undergo oxidation, and the partial oxidation without full mineralisation of such compounds results in k_{COD} higher than the k_{TOC}.

To assess the conditions to optimise the hydrogen generation in a membrane-less electrolyser (*i.e.* the operating conditions where the oxidation of the organics suppresses the OER), the ICE was calculated by equation **(2)** and reported in Fig. 9 as a function of the electrolysis time.

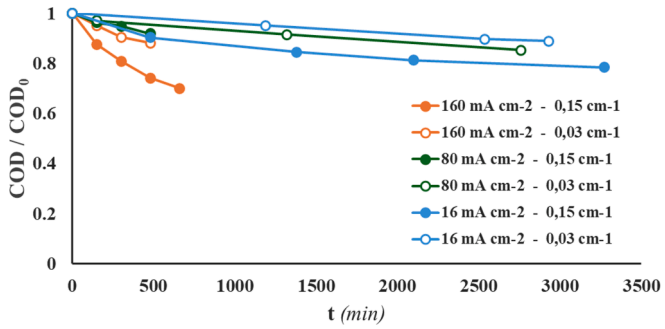

Fig. 8. Trend of normalised COD over time of al the galvanostatic electrolyses at all the explored conditions: 16, 80, 160 mA cm^{-2} at 0.03 and 0.15 cm^{-1}.

As shown, at 80 and 160 mA cm^{-2} and a = 0.15 cm^{-2}, ICE is lower than 100 %, while 100 % ICE is obtained with a = 0.03 cm^{-2} and J = 80 mA cm^{-2} in the first minutes of electrolysis. As it was observed for the mineralisation, also the operative conditions for complete suppression of OER depend on current density and organic load, as it is further confirmed by the very low values obtained with diluted wastewater (see **Figure S5**) also at 16 mA cm^{-2}.

With a current density of 16 mA cm^{-2}, ICE values of 100 % can be obtained with a = 0.15 and 0.03 cm^{-2}, indicating that the oxidation of the organics is the only reaction at the anode, *i.e.* the supplied charge is fully used for the oxidation of the organic load, and the OER is completely suppressed: ICE start to decrease under the 100 % value when about 10 % of COD is removed, as OER at the anode competes with the oxidation of the organics [40,41]. Thus, a = 0.03 cm^{-1} and J = 16 mA cm^{-2} represent the operating condition at which hydrogen is the only gaseous product, as the oxygen evolution is suppressed and the CO_2 produced by mineralisation of the organic load is absorbed in the liquid phase. To assess the potential of the process for hydrogen production during the treatment of real wastewater, specific experiments have been performed in an undivided filter-press-like cell inserted in a batch-recirculated hydraulic circuit with a = 0.03 cm^{-1}. Fig. 10 shows the hydrogen purity obtained during the first 15 min of electrolyses as a function of the applied current density. With a current density of 16 mA cm^{-2}, 100 % hydrogen was measured confirming the ability of the system to exploit the oxidation of organics to suppress the OER, so obtaining oxygen-free hydrogen with an undivided cell. As the current density increases, the gas produced contains oxygen other than hydrogen and a traditional two-camber cell should be used.

E_{EM} and E_{EO} (equations **(3) and (4)**) have been used as figures of merit to evaluate the energy consumptions using; E_{EM} was calculated for 25 % of COD removal, which was in turn calculated with equation (6) and the relevant k_{COD}. The values obtained are reported in Table 4 and shown in **Figure S6**a. The highest E_{EO} was obtained with a = 0.03 cm^{-1} and J = 160 mA cm^{-2}, while the E_{EM} presents a maximum at J = 80 mA cm^{-2}, as k_{COD} non-linearly increases with the applied current density. A similar behaviour has been found by Kumar and coworkers [42], where the E_{EM} values did not increase proportionally with the current density. Furthermore, energy consumption values are severely affected by ICE, since – under conditions where ICE < 100 % – also the side OER occurs. Based on the predicted E_{EM}, treating the tar-containing wastewater at the lowest current density (16 mA cm^{-2}) and at the higher a ratio (0.15 cm^{-1}) leads to 25 % COD removal with the lowest energy consumption (15.95 kWh kg^{-1}). Although a direct comparison of E_{EM} values with those reported in the literature is not straightforward due to different composition and concentration of the wastewaters, reactor geometries

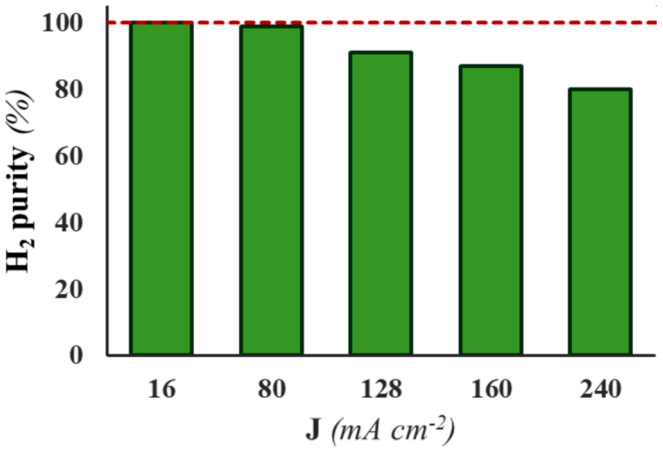

Fig. 10. Purity of the generated H_2 gas as a function of current density.

Table 4
Calculated E_{EO} and E_{EM} for the tar-containing wastewater for the relevant explored conditions.

a (cm^{-1})	J (mA cm^{-2})	E_{EO} (kWh m^{-3} $order^{-1}$)	E_{EM} (kWh kg^{-1})[a]
0.03	16	3438.53	35.59
0.03	80	14343.17	137.43
0.03	160	6925.47	70.97
0.15	16	1661.75	15.95
0.15	80	4726.15	48.53
0.15	160	2986.02	29.38

[a]Calculated at 25 % of removed COD.

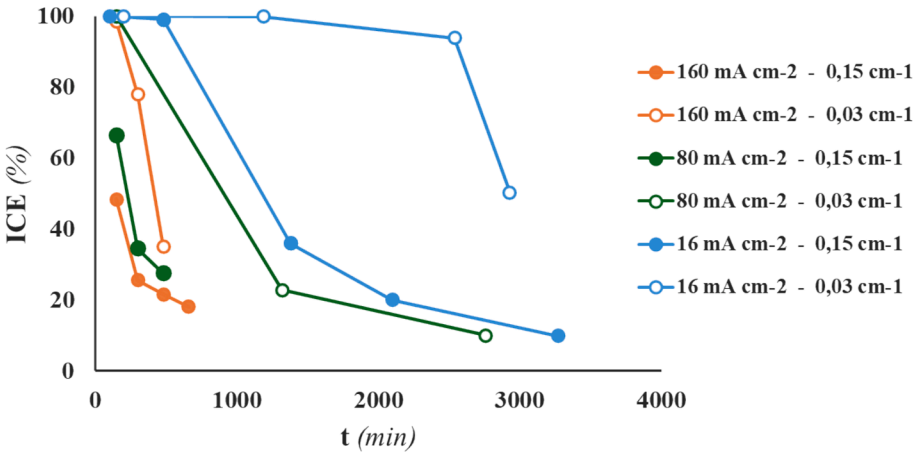

Fig. 9. Trend of ICE % with time for electrolyses of wastewater using 16, 80, 160 mA cm^{-2} at a = 0.03 and a = 0.15 cm^{-1}.

and electrode materials, the values calculated in this work are comparable with those obtained by other researchers. Yasuf *et al.* treated petroleum refinery wastewater with initial COD equal to 600 mg dm^{-3} using different electrode materials, reporting E_{EM} values up to over 30,000 kWh kg^{-1} with iron electrodes; conversely, much lower E_{EM} values, in the order of 3000 – 4000 kWh kg^{-1}, were noted with other electrode materials such as BDD [43]. Tien and coworkers performed the electrooxidation of tannery wastewater with a COD of around 4300 mg dm^{-3}, reporting E_{EC} values up to 180 kWh kg^{-1} depending on the applied current density, the electrode material and the COD removal [44]. Kumar *et al.* found an E_{EM} ranging from 100 to 600 kWh kg^{-1} of COD to treat a synthetic solution containing 100 – 300 mg dm^{-3} of nitrophenol with Ti/RuO_2 electrode similar to that used in this work [42].

E_{EO} values reported in the literature typically range from 10 to 2300 kWh m^{-3} $order^{-1}$, and a sharp increase in the energy consumption is observed when parasitic reactions reduce the overall treatment efficiency. Malpass *et al.* studied the treatment of a textile wastewater with different DSA-like electrode materials at different current densities. The authors reported E_{EO} values ranging from 320 to 2279 kWh m^{-3} $order^{-1}$ for the discoloration process, while the TOC removal was associated with E_{EM} values between 2950 and 7296 kWh kg^{-1}. Such high energy consumption values were attributed to the challenges inherent in treating real wastewater solutions [45].

As the E_{EO} is concerned, Vahid *et al.* compared various treatment methods for the degradation of C.I. Acid Blue 92 (AB92), a model azo dye, demonstrating 55.95 kWh m^{-3} $order^{-1}$ energy consumption using electrochemical oxidation [46]. Escudero *et al.* reported an energy consumption ranging from 56 to 310 kWh m^{-3} $order^{-1}$ for the electrochemical oxidation of a 50 mg dm^{-3} solution of *p*-cresol solution at different current densities. Notably, the highest E_{EO} was observed at the lowest current density [47].

The E_{EO} values obtained in this work are higher than that found in the literature; however, this parameter is highly influenced by the initial concentration, and it is usually suggested as a figure of merit for the evaluation of the energy consumption in diluted solution. Indeed, the corresponding E_{EO} values for the diluted tar wastewater are comparable with that form the literature ranging from about 90 to 2300 kWh m^{-3} $order^{-1}$ (see **Table S1** and **Figure S6**c-d).

4. Conclusions

In this work the electrochemical treatment of a wastewater from the clean-up system of a biomass gasifier has been studied. The process showed to be effective in treating the wastewater tested, with removal of aromatic fraction and phenols, and reduction of the whole organic load.

With a current density of 160 mA cm^{-2}, the phenols contained in the wastewater have been almost completely removed and a 30 % mineralisation has been achieved with a supplied charge of 350 Ah dm^{-3}. Moreover, the study provided insights into the kinetic aspects of the process, including the abatement of phenolic compounds and of the aromatic fraction of the solution.

The instantaneous current efficiency of process depended on organic load and current density, and the conditions for a 100 % yield for the removal of the organics have been identified, where only the reactions of oxidation of organics occur with no evolution of oxygen.

Under these conditions, the process could be used to recover hydrogen when treating the water in a undivided cell, with different advantages, including no ohmic losses due to the separator. Of note, the commercially available separators can be heavily damaged when a wastewater is used as electrolyte.

Although a complete techno-economic assessment of the wastewater treatment with simultaneous hydrogen recovery requires further investigation, some preliminary economic estimations can be done. The total annual cost of the treatment can be estimated from the cost breakdown of alkaline electrolysers, which can be considered as a parent technology of that tested in this work, such as that provided by the International Renewable Energy Agency [48]. The overall cost of the treatment can be obtained from the power supply that represent the 40 % of the overall costs of membrane-less electrolyser, while 27.5 % can be considered for an electrolyser with separator [48].

The lowest value of E_{EM} 15.95 kWh kg^{-1} obtained was 15.95 kWh kg^{-1} that corresponds to an energy consumption of 960 kWh m^{-3}. Considering an average energy price of electricity in Europe (year 2024) of 75 € MWh^{-1}, the power cost for the treatment is 72 € m^{-3}. Thus, the total cost for the process is 180 € m^{-3} (260 € m^{-3} with separator), that is comparable to costs reported in the literature for treatment of heavy-polluted wastewater.

CRediT authorship contribution statement

Nicola Melis: Writing – original draft, Methodology, Investigation. **Laura Mais:** Writing – original draft, Methodology, Investigation. **Michele Mascia:** Writing – review & editing, Methodology, Funding acquisition, Conceptualization. **Annalisa Vacca:** Writing – review & editing, Methodology, Funding acquisition, Conceptualization.

Declaration of competing interest

The authors declare that they have no known competing financial interests or personal relationships that could have appeared to influence the work reported in this paper.

Acknowledgements

This paper is part of the research project e.INS- (Ecosystem of Innovation for Next Generation Sardinia) funded by the Italian Ministry for Research and Education (MUR) within the Next generation EU framework (project code ECS 00000038). N. M. gratefully acknowledge the research project NEST (Network 4 Energy Sustainable Transition, project code MUR PE0000021) for funding his fellowship.

Appendix A. Supplementary data

Supplementary data to this article can be found online at https://doi.org/10.1016/j.cej.2024.156736.

Data availability

Data will be made available on request.

References

[1] R.C. Pietzcker, S. Osorio, R. Rodrigues, Tightening EU ETS targets in line with the European Green Deal: Impacts on the decarbonization of the EU power sector, Appl. Energy 293 (2021) 116914, https://doi.org/10.1016/j.apenergy.2021.116914.
[2] World Bioenergy Association, Global Bioenergy Statistics 2021, Stockholm, Sweden, 2021.
[3] J.B. Skjærseth, Towards a European Green Deal: The evolution of EU climate and energy policy mixes, Int. Environ. Agreem 21 (2021) 25–41, https://doi.org/10.1007/s10784-021-09529-4.
[4] Global Hydrogen Review 2021, Paris, 2021.
[5] A. Kovač, M. Paranos, D. Marciuš, Hydrogen in energy transition: A review, Int. J. Hydrogen Energy 46 (2021) 10016–10035, https://doi.org/10.1016/j.ijhydene.2020.11.256.
[6] M. Cortazar, L. Santamaria, G. Lopez, J. Alvarez, L. Zhang, R. Wang, X. Bi, M. Olazar, A comprehensive review of primary strategies for tar removal in biomass gasification, Energy Convers. Manag. 276 (2023) 116496, https://doi.org/10.1016/j.enconman.2022.116496.
[7] V. Mehta, A. Chavan, Physico-chemical treatment of tar-containing wastewater generated from biomass gasification plants, International Journal of Chemical, Molecular, Nuclear, Materials and Metallurgical Engineering 3 (2009) 59.
[8] A. Molino, S. Chianese, D. Musmarra, Biomass gasification technology: The state of the art overview, Journal of Energy Chemistry 25 (2016) 10–25, https://doi.org/10.1016/j.jechem.2015.11.005.
[9] N. Rakesh, S. Dasappa, A critical assessment of tar generated during biomass gasification - Formation, evaluation, issues and mitigation strategies, Renew.

Sustain. Energy Rev. 91 (2018) 1045–1064, https://doi.org/10.1016/j.rser.2018.04.017.
[10] L.P.L.M. Rabou, R.W.R. Zwart, B.J. Vreugdenhil, L. Bos, Tar in Biomass Producer Gas, the Energy research Centre of The Netherlands (ECN) Experience: An Enduring Challenge, Energy Fuel 23 (2009) 6189–6198, https://doi.org/10.1021/ef9007032.
[11] C. Font Palma, Modelling of tar formation and evolution for biomass gasification: A review, Appl. Energy 111 (2013) 129–141, https://doi.org/10.1016/j.apenergy.2013.04.082.
[12] R.J. Evans, T.A. Milne, Chemistry of Tar Formation and Maturation in the Thermochemical Conversion of Biomass, in: Developments in Thermochemical Biomass Conversion, Springer Netherlands, Dordrecht, 1997: pp. 803–816. 10.1007/978-94-009-1559-6_64.
[13] B. Zhou, A. Dichiara, Y. Zhang, Q. Zhang, J. Zhou, Tar formation and evolution during biomass gasification: An experimental and theoretical study, Fuel 234 (2018) 944–953, https://doi.org/10.1016/j.fuel.2018.07.105.
[14] A. Gredinger, R. Spörl, G. Scheffknecht, Comparison measurements of tar content in gasification systems between an online method and the tar protocol, Biomass Bioenergy 111 (2018) 301–307, https://doi.org/10.1016/j.biombioe.2017.01.026.
[15] Y. Ayub, J. Ren, T. Shi, Exploring gasification process and technology for biomass-waste utilization: A comprehensive review on the path to sustainable energy, Process Saf. Environ. Prot. 188 (2024) 1489–1501, https://doi.org/10.1016/j.psep.2024.06.056.
[16] Y. Yan, B. Lin, L. Zhang, Y. Wang, H. Zhang, H. Zheng, T. Zhou, Y. Zhan, Z. Yu, Y. Kuang, J. Tang, Electrochemical oxidation processes based on renewable energy towards carbon neutrality: Oxidation fundamentals, catalysts, challenges and prospects, Chem. Eng. J. 487 (2024) 150447, https://doi.org/10.1016/j.cej.2024.150447.
[17] W. Li, G. Song, J. Sun, M. Zhou, Electrochemical advanced oxidation processes towards carbon neutral wastewater treatment: A review, Chem. Eng. J. 480 (2024) 148044, https://doi.org/10.1016/j.cej.2023.148044.
[18] C.-G. Piuleac, C. Sáez, P. Cañizares, S. Curteanu, M.A. Rodrigo, Hybrid model of a wastewater-treatment electrolytic process, Int. J. Electrochem. Sci. 7 (2012) 6289–6301, https://doi.org/10.1016/S1452-3981(23)19481-8.
[19] A. MariaJoseph, S. Nangan, D. Verma, L. Gnanasekaran, S. Rajendran, T. Natesan, P. Pattananuwat, M. Okhawilai, Rational coupling of selective electrochemical oxidation and reduction reactions for in-situ value-added chemical generation, Fuel 367 (2024) 131408, https://doi.org/10.1016/j.fuel.2024.131408.
[20] W. Xi, P. Yang, M. Jiang, X. Wang, H. Zhou, J. Duan, M. Ratova, D. Wu, Electrochemical CO2 reduction coupled with alternative oxidation reactions: Electrocatalysts, electrolytes, and electrolyzers, Appl. Catal. B 341 (2024) 123291, https://doi.org/10.1016/j.apcatb.2023.123291.
[21] P. Cañizares, R. Paz, C. Sáez, M.A. Rodrigo, Electrochemical Oxidation of Wastewaters Polluted with Aromatics and Heterocyclic Compounds, J. Electrochem. Soc. 154 (2007) E165, https://doi.org/10.1149/1.2772415.
[22] P. Cañizares, J. Lobato, R. Paz, M. Rodrigo, C. Sáez, Electrochemical oxidation of phenolic wastes with boron-doped diamond anodes, Water Res. 39 (2005) 2687–2703, https://doi.org/10.1016/j.watres.2005.04.042.
[23] S. Zhang, W. Leng, S. Zhang, H. Lu, X. Xu, Z. Zang, D. Wu, In-situ active sites analysis of bifunctional metal-organic frameworks for coupled adsorption and electrochemical oxidation of PPCPs, Chem. Eng. J. 486 (2024) 150322, https://doi.org/10.1016/j.cej.2024.150322.
[24] D. Rajkumar, K. Palanivelu, Electrochemical Degradation of Cresols for Wastewater Treatment, Ind. Eng. Chem. Res. 42 (2003) 1833–1839, https://doi.org/10.1021/ie020759e.
[25] A.S. Fajardo, H.F. Seca, R.C. Martins, V.N. Corceiro, I.F. Freitas, M.E. Quinta-Ferreira, R.M. Quinta-Ferreira, Electrochemical oxidation of phenolic wastewaters using a batch-stirred reactor with NaCl electrolyte and Ti/RuO2 anodes, J. Electroanal. Chem. 785 (2017) 180–189, https://doi.org/10.1016/j.jelechem.2016.12.033.
[26] Q. Zhao, F. Wei, L. Zhang, Y. Yang, S. Lv, Y. Yao, Electrochemical oxidation treatment of coal tar wastewater with lead dioxide anodes, Water Sci. Technol. 80 (2019) 836–845, https://doi.org/10.2166/wst.2019.323.
[27] N. Yu, J. Wei, Z. Gu, H. Sun, Y. Guo, J. Zong, X. Li, P. Ni, E. Han, Electrocatalysis degradation of coal tar wastewater using a novel hydrophobic benzalacetone modified lead dioxide electrode, Chemosphere 289 (2022) 133014, https://doi.org/10.1016/j.chemosphere.2021.133014.
[28] Y. Chen, Y. Fu, W. Peng, S. Wang, Minireview of Coupled Electrochemical Hydrogen Production and Organic-Oxidation for Low Energy Consumption, Energy Fuel 37 (2023) 17915–17931, https://doi.org/10.1021/acs.energyfuels.3c02539.
[29] R. Núñez, N. Merayo, D. Hermosilla, A. Gascó, A.J. Dos santos-García, Á. Caravaca, Electrochemical treatment of industrial wastewater for hydrogen production, Curr Opin, Electrochem 46 (2024) 101533, https://doi.org/10.1016/j.coelec.2024.101533.
[30] B. Mahjoub, E. Jayr, R. Bayard, R. Gourdon, Phase partition of organic pollutants between coal tar and water under variable experimental conditions, Water Res. 34 (2000) 3551–3560, https://doi.org/10.1016/S0043-1354(00)00100-7.
[31] R. Kothari, D. Buddhi, R. Sawhney, Optimization of electrolytic input power for the production of hydrogen, Int. J. Hydrogen Energy 31 (2006) 2329–2336, https://doi.org/10.1016/j.ijhydene.2006.02.021.
[32] L. Vernasqui, M.A. Montiel, N. Gomes Ferreira, P. Cañizares, M.A. Rodrigo, Design, validation, and fabrication of a tailored electrochemical reactor using 3D printing for studies of commercial boron-doped diamond electrodes, Ind. Eng. Chem. Res. 63 (2024) 5488–5498, https://doi.org/10.1021/acs.iecr.3c03123.
[33] M. Ettinger, C. Ruchhoft, R. Lishka, Sensitive 4-aminoantipyrine method for phenolic compounds, Anal. Chem. 23 (1951) 1783–1788, https://doi.org/10.1021/ac60060a019.
[34] M. Nataraja, Y. Qin, E.A. Seagren, Ultraviolet spectrophotometry as an index parameter for estimating the biochemical oxygen demand of domestic wastewater, Environ. Technol 27 (2006) 789–800, https://doi.org/10.1080/09593332708618691.
[35] A.J. Bard, L.R. Faulkner, Electrochemical Methods: Fundamental and Applications, 2nd ed., John Wiley & Sons Inc, 2001.
[36] J.R. Bolton, K.G. Bircher, W. Tumas, C.A. Tolman, Figures-of-merit for the technical development and application of advanced oxidation technologies for both electric- and solar-driven systems (IUPAC Technical Report), Pure Appl. Chem. 73 (2001) 627–637, https://doi.org/10.1351/pac200173040627.
[37] N. Elgrishi, K.J. Rountree, B.D. McCarthy, E.S. Rountree, T.T. Eisenhart, J. L. Dempsey, A Practical Beginner's Guide to Cyclic Voltammetry, J. Chem. Educ 95 (2018) 197–206, https://doi.org/10.1021/acs.jchemed.7b00361.
[38] A.K. Singh, D. Kumar, B. Singh, A. Indra, Replacing anodic oxygen evolution reaction with organic oxidation: the importance of metal (oxy)hydroxide formation as the active oxidation catalyst, Synlett 34 (2023) 552–560, https://doi.org/10.1055/a-1894-8136.
[39] X. Li, Y. Cui, Y. Feng, Z. Xie, J.-D. Gu, Reaction pathways and mechanisms of the electrochemical degradation of phenol on different electrodes, Water Res. 39 (2005) 1972–1981, https://doi.org/10.1016/j.watres.2005.02.021.
[40] A. Kapałka, G. Fóti, C. Comninellis, Kinetic modelling of the electrochemical mineralization of organic pollutants for wastewater treatment, J. Appl. Electrochem. 38 (2007) 7–16, https://doi.org/10.1007/s10800-007-9365-6.
[41] A. Urtiaga, P. Gómez, A. Arruti, I. Ortiz, Electrochemical removal of tetrahydrofuran from industrial wastewaters: anode selection and process scale-up, J. Chem. Technol. Biotechnol. 89 (2014) 1243–1250, https://doi.org/10.1002/jctb.4384.
[42] S. Kumar, S. Singh, V.C. Srivastava, Electro-oxidation of nitrophenol by ruthenium oxide coated titanium electrode: Parametric, kinetic and mechanistic study, Chem. Eng. J. 263 (2015) 135–143, https://doi.org/10.1016/j.cej.2014.11.051.
[43] Y. Yavuz, A.S. Koparal, Ü.B. Öğütveren, Treatment of petroleum refinery wastewater by electrochemical methods, Desalination 258 (2010) 201–205, https://doi.org/10.1016/j.desal.2010.03.013.
[44] T.T. Tien, T. Le Luu, Electrooxidation of tannery wastewater with continuous flow system: Role of electrode materials, Environ. Eng. Res. 25 (2019) 324–334, https://doi.org/10.4491/eer.2018.349.
[45] G.R.P. Malpass, D.W. Miwa, S.A.S. Machado, A.J. Motheo, Decolourisation of real textile waste using electrochemical techniques: Effect of electrode composition, J. Hazard. Mater. 156 (2008) 170–177, https://doi.org/10.1016/j.jhazmat.2007.12.017.
[46] B. Vahid, A. Khataee, Photoassisted electrochemical recirculation system with boron-doped diamond anode and carbon nanotubes containing cathode for degradation of a model azo dye, Electrochim Acta 88 (2013) 614–620, https://doi.org/10.1016/j.electacta.2012.10.069.
[47] C.J. Escudero, O. Iglesias, S. Dominguez, M.J. Rivero, I. Ortiz, Performance of electrochemical oxidation and photocatalysis in terms of kinetics and energy consumption. New insights into the p-cresol degradation, J Environ Manage 195 (2017) 117–124, https://doi.org/10.1016/j.jenvman.2016.04.049.
[48] IRENA, Green Hydrogen Cost Reduction: Scaling up Electrolysers to Meet the 1.5°C Climate Goal, 2020.